A Low-Complexity Frame Synchronization and Frequency Offset Compensation Scheme for OFDM Systems over Fading Channels

Meng-Han Hsieh, *Student Member, IEEE,* and Che-Ho Wei, *Fellow, IEEE*

***Abstract*— This paper presents a fast low-complexity synchronization scheme for orthogonal frequency division multiplexing (OFDM) systems over fading channels. By utilizing the guard interval in OFDM signals, the frame synchronization and the frequency offset estimation are considered simultaneously. The implementation can be simplified by only using the sign bits of the in-phase and the quadrature components of the received OFDM signal for frame synchronization and frequency offset compensation. A frequency-offset independent frame synchronization algorithm is derived, and a low-complexity frequency offset estimator based on the synchronized correlator output is presented in this paper. Due to the subcarrier ambiguity in the guard-interval-based (GIB) frequency detector, the maximum correctable frequency range is limited to $\pm 1/2$ of the subcarrier spacing. In this paper, we also present a new frequency acquisition scheme that can solve the subcarrier ambiguity problem and extend the frequency acquisition range to nearly a half of the useful OFDM signal bandwidth.**

***Index Terms*— Frame synchronization, frequency offset compensation, low-complexity algorithms, OFDM.**

I. Introduction

THE ORTHOGONAL frequency division multiplexing (OFDM) technique is an effective transmission scheme to cope with many channel impairments, such as cochannel interference, severe multipath fading, and impulsive parasitic noise [1]. By inserting a guard interval between symbol blocks, the intersymbol interference (ISI) in an OFDM system can be mitigated.

For block transmission of the OFDM signals, a frame synchronization is needed to detect the proper time instant to start sampling a new frame. A popular solution for the frame synchronization is to insert some synchronization symbols within the OFDM signals as the pilot symbols [2]. These symbols are then picked up by the receiver to generate the frame clock. However, the insertion of the pilot symbols decreases the system capacity. For nondata-aided frame synchronization, a guard-interval-based (GIB) low-complexity frame synchronization scheme has been presented in [3] to estimate the start position of a new frame. The basic idea of this scheme is to exploit the cyclic extension preceding a symbol frame, known as guard interval. This scheme only uses the in-phase and the quadrature sign bits of the OFDM data to estimate the frame position. If the channel is time dispersive, the intersymbol interference will introduce errors in the frame synchronization scheme. In this paper, the influence of the frame position error on the symbols at the fast Fourier transform (FFT) output is investigated and some modifications of the conventional frame synchronization schemes are also made.

In the practical OFDM systems, a frequency offset due to the Doppler effect or the oscillator mismatching usually exists between the transmitter and the receiver. The frame synchronization scheme presented in [3] may not work properly under such condition. After some modifications of the original scheme, we derive a frame synchronization scheme that is independent of the frequency offset.

To compensate the carrier frequency offset, several data-aided frequency offset correction techniques have been proposed [4], [5], [7], [12]. Although those algorithms estimate the frequency offset accurately, the data-aided structure limits their applicable field because some specialized synchronization symbols must be generated in the transmitter side. For the nondata-aided frequency offset compensation algorithms, some GIB frequency detectors have been presented in [6] and [10]. In [6], only the last few samples in the guard interval are used to estimate the frequency offset, therefore, the estimate is sensitive to the frame synchronization error. In [10], timing recovery and carrier recovery are implemented by a maximum-likelihood estimator based on the guard interval samples, but the computational complexity is high. Similar to the estimator in [10], we estimate the start position of the frame and the carrier frequency offset at the same time. However, unlike the maximum-likelihood estimator proposed in [10], only the sign bits of the in-phase component and the quadrature component of the received signal are used to estimate the frequency offset, therefore the complexity is reduced drastically. By averaging the estimate over a few frames or by using a closed tracking loop, a more accurate frequency offset estimation scheme can be obtained. Since only adders and buffers are required in our synchronization scheme, we can estimate the frequency offset and the frame position for each frame with low computational complexity. Even in slow fading environment, the frequency offset can be accurately tracked.

On the other hand, the subcarrier ambiguity problem will limit the correctable frequency offset range within $\pm 1/2$ sub-

Manuscript received February 24, 1997; revised August 19, 1998. This work was supported by the National Science Council of the Republic of China under Grant NSC86-2221-E-009-059.

The authors are with the Department of Electronics Engineering, National Chiao Tung University, Hsin Chu, Taiwan, R.O.C. (e-mail: meng@clab.ee.nctu.edu.tw; chwei@cc.nctu.edu.tw).

Publisher Item Identifier S 0018-9545(99)07395-8.

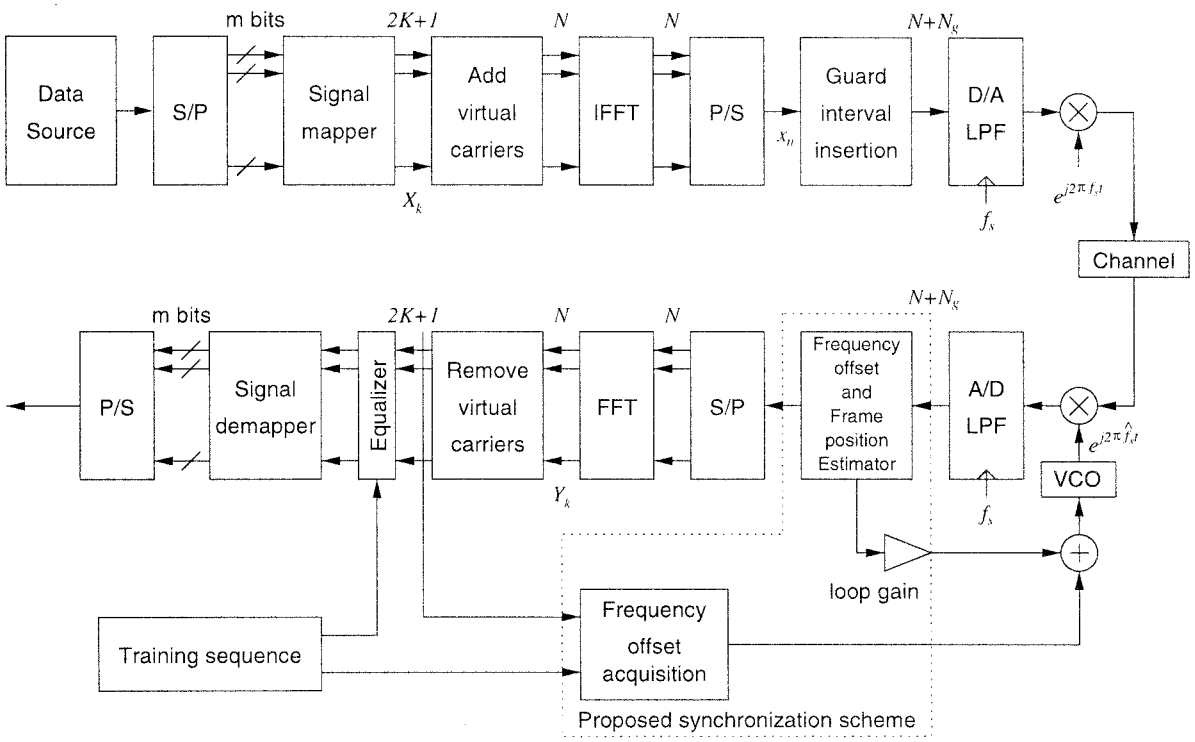

Fig. 1. OFDM system with synchronization scheme.

channel bandwidth [4], [6]. Several frequency offset acquisition schemes have been mentioned for some specific frequency detectors [4], [5], [7]. A data-aided frequency acquisition scheme has also been proposed in [8], which uses a particular synchronization symbol to acquire the frequency offset. Here, we present a frequency acquisition scheme adopted from [11] to extend the acquisition range of the GIB frequency detector from $\pm 1/2$ of the subcarrier spacing to a large fraction of the signaling rate. Since the training sequences of the frequency domain equalization are used to acquire the carrier frequency offset, no additional synchronization symbols are needed. The influence of the frequency detection error on the frequency acquisition scheme is also discussed in this paper.

This paper is organized as follows. Section II introduces basic OFDM systems and the low-complexity frame synchronization scheme based on the analysis of the guard intervals. The analysis work and the simulation results for several averaging schemes are also included in this section. Section III presents a new GIB synchronization scheme that can estimate the carrier frequency offset and the frame position simultaneously. Section IV introduces the frequency acquisition scheme based on the frequency detector presented in the previous section. Finally, Section V gives some conclusions.

II. Frame Synchronization Scheme

We consider the frame synchronization problem in the transmission system based on the OFDM technique. The block diagram of a typical OFDM system is shown in Fig. 1. The transmitted baseband signal $\{x_n\}$ is composed of $2K+1$ complex sinusoids modulated with $2K+1$ complex modulation values $\{X_k\}$, i.e.,

$$x_n = \left(\frac{1}{N}\right) \sum_{k=-K}^{K} X_k e^{2\pi jnk/N}, \quad n = 0, \cdots, N-1;\ N \geq 2K+1. \tag{1}$$

We note that the N-point discrete Fourier transform (DFT) of (1) is the N-point sequence

$$\begin{aligned} &\mathrm{DFT}_N\{x_n\} \\ &\quad = \left\{ \sum_{n=0}^{N-1} x_n e^{-2\pi jnk/N} \right\}_{k=-K,\,-K+1,\,\cdots,\,K-1,\,K} \\ &\quad = \{X_0, X_1, \cdots, X_K, 0, 0, \cdots, 0, X_{-K}, \cdots, \\ &\qquad X_{-2}, X_{-1}\} \end{aligned} \tag{2}$$

of modulation values, and the zeros in (2) are the virtual carriers. Thus, if the orthogonality within each OFDM block is preserved, the data $\{X_k\}$ can be recovered in the receiver by a DFT.

In time-dispersive channels, the intersymbol interference caused by the multipath effect induces a loss in orthogonality of OFDM signals. To maintain the orthogonality of OFDM signals in multipath channels, a guard interval is inserted in front of each OFDM block. The guard interval insertion duplicates the last N_g samples of $\{x_n\}$ and appends them as a preamble (cyclic prefix) to form an OFDM frame $\{s_k\}$. As a result, the actual transmitted signal is not a white process.

In [3], van de Beek *et al.* presented a low-complexity frame synchronization based on the inherent correlation property of the OFDM signals with guard interval. The block diagram of their frame synchronization scheme is shown in Fig. 2. The in-phase and the quadrature components of the received

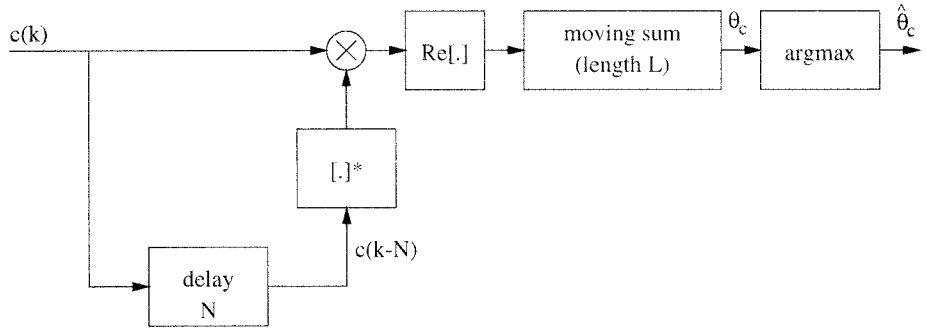

Fig. 2. Block diagram of a low-complexity ML estimator for frame synchronization [3].

signal $r(k)$ are quantized to $c(k)$. For the sake of reducing the complexity, only sign bits of the in-phase and the quadrature components are used. The OFDM signal in Fig. 2 can be processed continuously. The output sequence of the moving sum is a concatenation of loglikelihood functions for consecutive OFDM frames.

Next, we investigate the influence of the frame errors on the FFT output symbols while additive white Gaussian noise (AWGN) channel is used. If the estimated start position of the frame is located within the guard interval, each FFT output symbol within the frame will be rotated by a different angle. From subcarrier to subcarrier, the angle increases proportionally to the frequency offset. If the estimated start position of the frame locates within the data interval, the sampled OFDM frame will contain some samples that belong to other OFDM frame. Therefore, each symbol at the FFT output is rotated and dispersed due to the intersymbol interference from other OFDM frame. The phase rotation imposed by frame synchronization error can thus be corrected by appropriately rotating the received signal, but the dispersion of signal constellation caused by ISI forms a bit error rate (BER) floor. Another effect that we must take into account is the channel impairment. The OFDM symbols are dispersed in time axis due to the multipath effect. Consequently, the guard interval used to estimate the frame location is interfered by the previous symbol.

A solution to remedy this problem is to use different smoothing algorithms in place of the moving sum scheme shown in Fig. 2. Instead of using the moving sum shown in Fig. 2 that weights $\mathrm{Re}\{c(k)\cdot c^*(k-N)\}$ equally, an exponentially decaying weighted function is applied to $\mathrm{Re}\{c(k)\cdot c^*(k-N)\}$. We consider four smoothing algorithms here. Let L be the number of samples in a guard interval, the loglikelihood functions at time instant θ_c for these algorithms are given as follows.

Moving average (MA):

$$\Lambda_c(\theta_c)=\sum_{k=\theta_c-L+1}^{\theta_c}\mathrm{Re}\{c(k)c^*(k-N)\}. \tag{3}$$

Shortened moving average (SMA):

$$\Lambda_c(\theta_c)=\sum_{k=\theta_c-L'+1}^{\theta_c}\mathrm{Re}\{c(k)c^*(k-N)\},\quad \text{where } L'\le L. \tag{4}$$

Exponentially weighted moving average (EWMA):

$$\Lambda_c(\theta_c)=\sum_{k=\theta_c-L+1}^{\theta_c}w^{\theta_c-k}\,\mathrm{Re}\{c(k)c^*(k-N)\}. \tag{5}$$

Exponentially weighted average (EWA):

$$\Lambda_c(\theta_c)=\sum_{k=0}^{\theta_c}w^{\theta_c-k}\,\mathrm{Re}\{c(k)c^*(k-N)\}. \tag{6}$$

Note that the moving average (MA) scheme is identical to the moving sum scheme presented in [3]. The MA, SMA, and EWMA algorithms can be realized as FIR filters, and the EWA algorithm can be realized as an IIR filter.

Computer simulations are used to evaluate these four averaging schemes. The wireless urban channel adopted by [6] is used and a complex white Gaussian noise is added to the received OFDM signals. The signal-to-noise ratio (SNR) is set to 10 dB. The delay spread of the multipath channel used in our simulation is about 5 μs. An OFDM system consisting of 1024 subcarriers with a guard interval having $L=128$ samples is employed. The sampling frequency is 9 MHz and the symbol rate is $8\cdot 10^6$ symbols/s. The probability of the estimated frame position obtained from the low-complexity frame synchronization scheme with various averaging schemes are shown in Fig. 3. For each case, 20 000 frames are simulated. Three different window lengths, 32, 64, and 96 samples, are employed to the SMA scheme. The weighting factor w for both EWMA scheme and EWA scheme is intentionally chosen such that $w=1-2^{-M}$, where M is a positive integer. By appropriately choosing the weighting factor, the multiplication operation within the summing scheme can be replaced by an adder and a shifter. Three different weighting factors employed in the simulations are expressed by $w=1-2^{-M}$, where $M=4$, 6, and 8.

As shown in Fig. 3, the three modified frame synchronization schemes have more concentrated probability distributions than the MA scheme over the multipath fading channel by appropriately choosing L' and w. We also notice that the modified frame synchronization schemes tend to estimate the frame start position within the guard interval and hence produce less ISI. Fig. 3(a) shows that if the window length L'

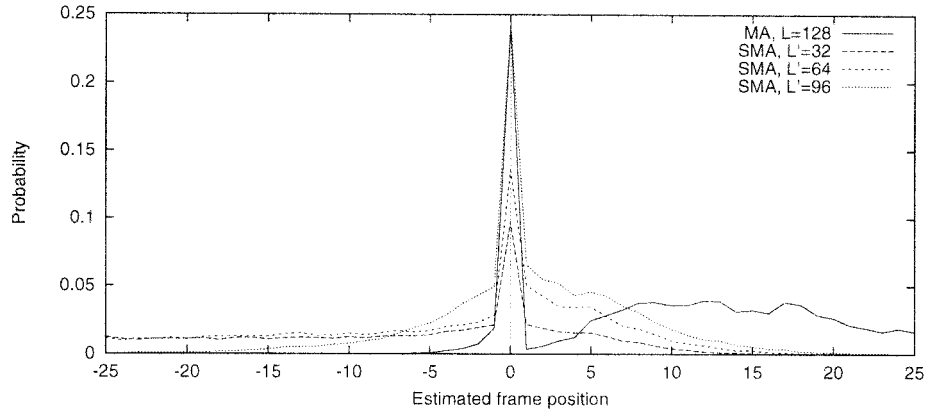

(a)

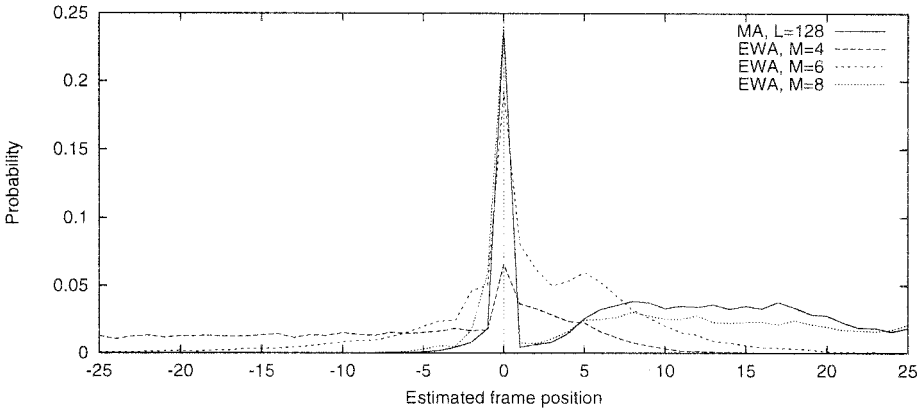

(b)

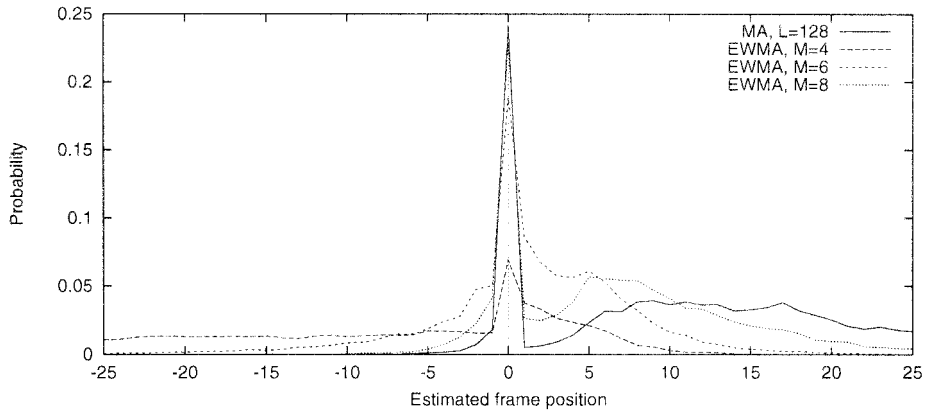

(c)

Fig. 3. Probability of estimated frame position: (a) moving average scheme and shortened moving average (SMA) scheme, (b) moving average scheme and exponentially weighted moving average (EWMA) scheme with weighting factor $w = 1 - 2^{-M}$, $M = 4, 6, 8$, and (c) moving average scheme and EWA scheme with weighting factor $w = 1 - 2^{-M}$, $M = 4, 6, 8$.

of SMA scheme is too small, the probability distribution of the estimated frame position will disperse. Also, if the weighting factor w is too large, the probability distribution of the EWA scheme will disperse and the residual tails will introduce ISI, as shown in Fig. 3(c). The EWMA scheme has no such problem because the correlated values $c(k) \cdot c^*(k-N)$ output from the buffer are discarded. For small w, the weight decays faster and the effective SNR for estimating the frame position is smaller; and thus, the probability distribution disperses. Comparing Fig. 3(b) with (c), we can see that, if w is not too large, the probability distribution of the EWMA scheme is almost the same as the probability distribution of the EWA scheme. Therefore, for smaller $w = 1 - 2^{-M}$ ($M < 7$), we can use the EWA scheme instead of the EWMA scheme to reduce the complexity. From our experimental results shown in Fig. 3, a window length $L' = 96$ for SMA scheme and a weighting factor $w = 1 - 2^{-6} = 0.984\,375$ for EWA and EWMA are suitable choices for the urban channel. However, the EWA

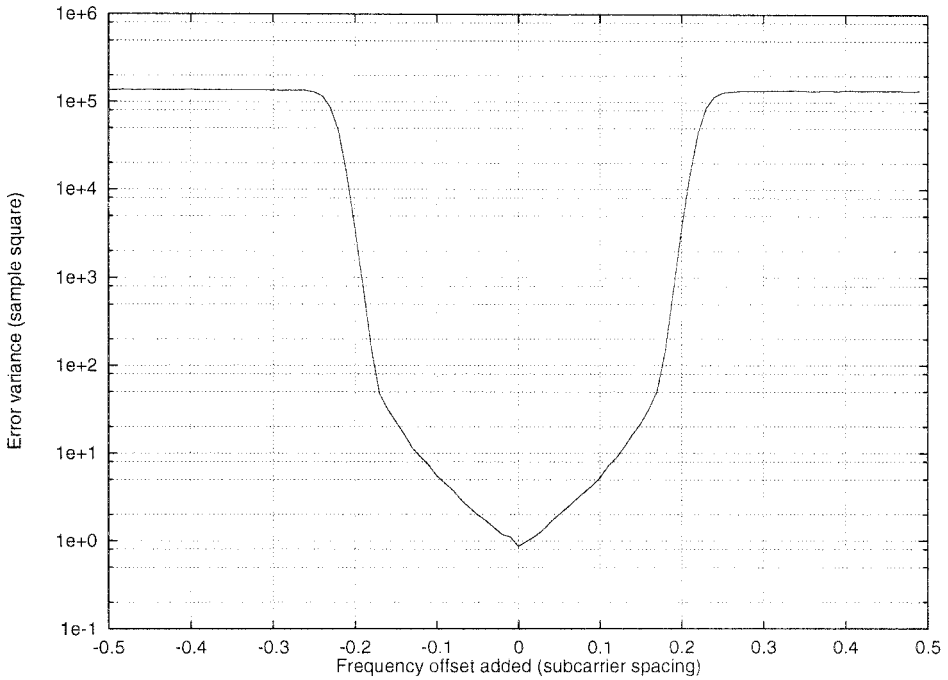

Fig. 4. Error variance of low-complexity frame synchronizer with various frequency offsets under AWGN channel, SNR = 25 dB.

scheme is more preferable because of its simpler hardware structure for practical implementation.

III. Low-Complexity Frequency Offset Correction Scheme

In OFDM systems, a carrier frequency error often exists between the transmitter and the receiver due to the mismatch between the oscillators or the Doppler effect in mobile radio channels. The carrier frequency offset introduces intercarrier interference (ICI) in OFDM systems and reduces the orthogonality between the different subcarriers which assemble the OFDM signal and, thus, degrades the overall system performance. For the OFDM signals constructed by many orthogonal subcarriers, the subchannel bandwidth is much smaller than the total bandwidth. As described in [4], a small frequency offset in the OFDM system will lead to a substantial SNR degradation.

The frequency error in an OFDM system is often corrected by a tracking loop with a frequency detector to estimate the frequency offset. In the literature, several algorithms have been proposed to estimate the frequency offset and can be classified into three categories:

1) algorithms based on the analysis of special synchronization blocks embedded in the OFDM temporal frame (data-aided) [4], [7];
2) algorithms based on the analysis of the received data at the output of the FFT (nondata-aided) [5], [12];
3) algorithms based on the analysis of the sampled received signal before the FFT block and making use of the redundancy introduced by the inserted guard interval in the OFDM signal frame (GIB) [6], [10].

The algorithms belonging to the first category require special synchronization blocks to estimate the frequency offset, but they provide better results. Since the insertion of synchronization blocks will lower the information rate, the number of synchronization blocks must be small comparing to the number of data blocks. The first category of algorithms estimates the frequency offset only when the synchronization block is received, as a result, the acquisition time for these algorithms is longer. Furthermore, the nonlinearity of the channel increases the estimation complexity. The algorithms in the second category do not need special synchronization blocks, but the performance is poor, especially in the mobile radio environments. The last category of algorithms utilizes the inherent data property of the OFDM signals and achieves synchronization accurately. The computational complexity of the algorithms in the last category are comparatively lower than those in the other two categories.

The GIB frequency detector in [6] uses the last few samples of a guard interval to estimate the frequency offset, therefore, a small frame synchronization error will induce deleterious effect on the GIB frequency detector. As the frame error interferes the GIB frequency detector, the frequency offset also militates against the GIB frame synchronization scheme. A simulation is conducted to illustrate the impact of the frequency offset on the frame synchronization scheme. An OFDM system consisting of 1024 subcarriers with a guard space of 128 samples over AWGN channel is considered. The SNR is set to 25 dB, and we estimate the error variance $E\{(\hat{\theta}-\theta)^2\}$ as a function of the normalized frequency offset. For each frequency offset value, 10 000 frames are simulated. From Fig. 4, we can see that the frequency offset affects the GIB frame estimation considerably.

To ensure the low-complexity frame synchronization scheme to work properly in an OFDM system with carrier frequency error, the frame position and the frequency

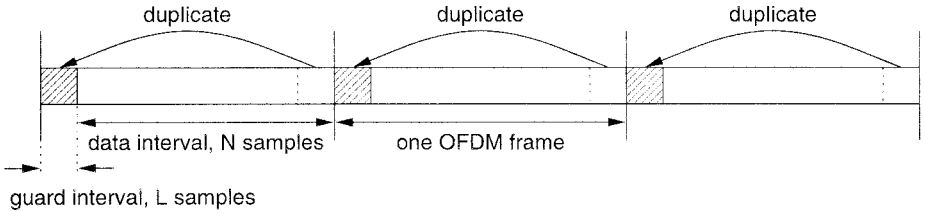

Fig. 5. OFDM signals with guard interval inserted.

offset must be estimated simultaneously. The guard interval generated by duplicating the last L samples of an OFDM block is placed in front of this block as shown in Fig. 5. The duration of the guard interval should be greater than the channel impulse response to eliminate the intersymbol interference (ISI) effect. Let $\mathcal{I}$ be a set that contains the last L samples of an OFDM frame, $\mathcal{I}'$ represent the cyclic prefix (guard interval) which is a replica of $\mathcal{I}$. Given the observations $r(k)$, $k = 1, \cdots, 2N + L$, the loglikelihood function without frequency offset at the time instant θ is given by [3]

$$\Lambda_r(\theta) = \sum_{k=\theta-L+1}^{\theta} 2(1-\rho)\,\mathrm{Re}\{r(k)\cdot r^*(k-N)\} - \rho\cdot|r(k)-r(k-N)|^2 \tag{7}$$

where

$$\rho = \frac{E\{|s(k)|^2\}}{E\{|s(k)|^2\}+E\{|n(k)|^2\}} = \frac{\mathrm{SNR}}{\mathrm{SNR}+1} \tag{8}$$

is the correlation coefficient of the sample $r(k) \in \mathcal{I}$, and the sample $r(k-N)$ in the cyclic prefix. If a residual frequency error exists between the transmitter and the receiver local oscillators, the phase of the correlated value $r(k)\cdot r^*(k-N)$ in (7) will be rotated with a certain amount.

Assuming that the frequency offset between the receiver and the transmitter is ϵ subcarrier spacing units, the loglikelihood function at the time instant θ can be extended from (7) as

$$\begin{aligned}\Lambda_r(\theta,\epsilon) &= \sum_{k=\theta-L+1}^{\theta} 2(1-\rho)\,\mathrm{Re}\{r(k)\cdot e^{j2\pi\epsilon}\cdot r^*(k-N)\} - \rho\cdot|r(k)\cdot e^{j2\pi\epsilon}-r(k-N)|^2 \\ &= \sum_{k=\theta-L+1}^{\theta}[e^{j2\pi\epsilon}\cdot r(k)\cdot r^*(k-N)+e^{-j2\pi\epsilon}\cdot r^*(k)\cdot r(k-N)] - \rho\cdot\sum_{k=\theta-L+1}^{\theta}[r(k)\cdot r^*(k)+r(k-N)\cdot r^*(k-N)].\end{aligned} \tag{9}$$

By taking the partial derivative of the loglikelihood function with respect to ϵ, we have

$$\frac{\partial\Lambda_r(\theta,\epsilon)}{\partial\epsilon} = j2\pi\cdot\sum_{k=\theta-L+1}^{\theta}[r(k)\cdot r^*(k-N)e^{j2\pi\epsilon} - r^*(k)\cdot r(k-N)e^{-j2\pi\epsilon}]. \tag{10}$$

To derive ϵ that maximizes $\Lambda_r(\theta,\epsilon)$, the partial derivative is set to zero, and the following equation is obtained:

$$e^{j2\pi\hat{\epsilon}} = C\cdot\sum_{k=\theta-L+1}^{\theta} r^*(k)\cdot r(k-N) \tag{11}$$

where

$$C = \frac{1}{\left|\sum_{k=\theta-L+1}^{\theta} r^*(k)\cdot r(k-N)\right|} \tag{12}$$

is a positive scaling factor. Consequently, the maximum likelihood estimate of the frequency offset is given by

$$\begin{aligned}\hat{\epsilon} &= \frac{1}{2\pi}\angle\left(\sum_{k=\theta-L+1}^{\theta} r(k)\cdot r^*(k-N)\right) \\ &= \frac{1}{2\pi}\tan^{-1}\frac{\sum_{k=\theta-L+1}^{\theta}\mathrm{Im}\{r(k)\cdot r^*(k-N)\}}{\sum_{k=\theta-L+1}^{\theta}\mathrm{Re}\{r(k)\cdot r^*(k-N)\}}.\end{aligned} \tag{13}$$

This estimate is similar to that of the frequency estimator proposed in [4]. It is noted that the maximum-likelihood estimate for the frequency offset is independent of the noise power.

A low-complexity frequency estimator can be obtained by replacing $r(k)$ and $r(k-N)$ with their quantized version $c(k)$ and $c(k-N)$, respectively. Then, a low-complexity frequency estimator is obtained with

$$\hat{\epsilon}_c = \frac{1}{2\pi}\tan^{-1}\frac{\sum_{k=\theta-L+1}^{\theta}\mathrm{Im}\{c(k)\cdot c^*(k-N)\}}{\sum_{k=\theta-L+1}^{\theta}\mathrm{Re}\{c(k)\cdot c^*(k-N)\}}. \tag{14}$$

From (14), we also notice that the start position θ of the frame should be given to estimate the frequency offset. The primary effect of the frequency offset to the low-complexity frame synchronization scheme is phase rotation. Therefore, we can use the amplitude of $\sum_{k=\theta-L+1}^{\theta} c(k)\cdot c^*(k-N)$ instead of its real part to estimate θ. A simpler way to estimate θ is to find the maximal sum of the absolute value of the real part and the imaginary part of $\sum_{k=\theta-L+1}^{\theta} c(k)\cdot c^*(k-N)$. The

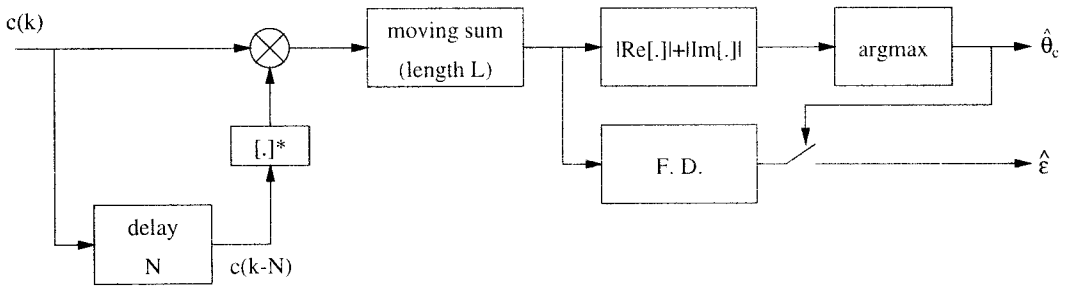

Fig. 6. System block diagram of the ML estimator for frequency offset and frame position.

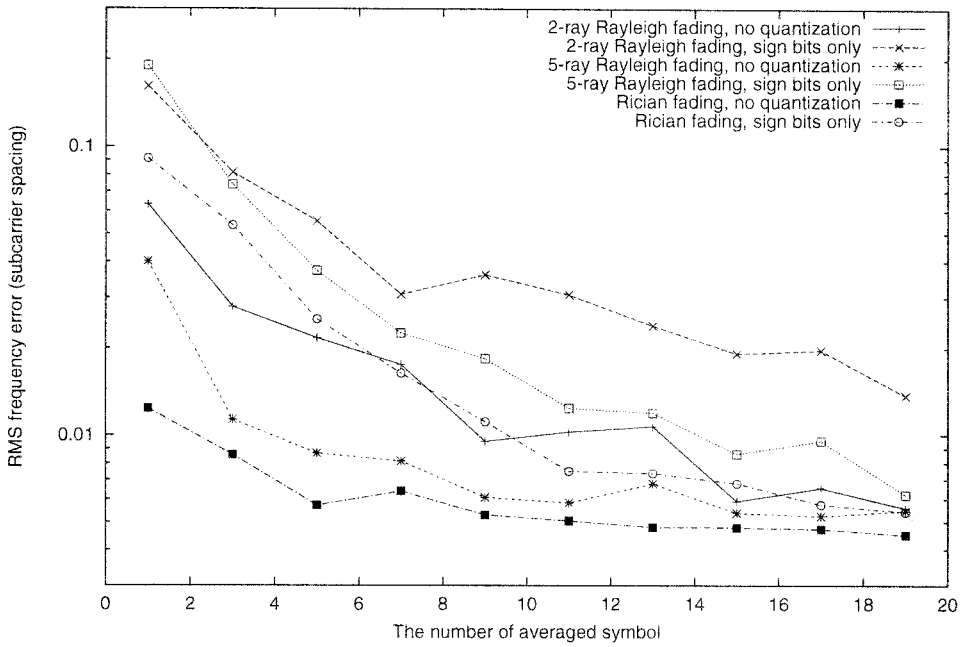

Fig. 7. RMS frequency error versus the number of averaged symbols.

frame position estimator thereby becomes

$$\hat{\theta}_c = \underset{\theta}{\operatorname{argmax}} \sum_{k=\theta-L+1}^{\theta} |\mathrm{Re}\{c(k)c^*(k-N)\}| + |\mathrm{Im}\{c(k)c^*(k-N)\}|. \quad (15)$$

Fig. 6 shows the functional block diagram of the estimator. The estimator detects the frame start position and the frequency offset error at the same time. To obtain a more accurate estimate, we can average the estimate over several OFDM symbols.

Fig. 7 shows the root-mean-square value of the residual frequency error from our simulations. The parameters of the simulated OFDM system are listed in Table I. Three channel models, Rician channel, two-ray Rayleigh fading channel, and five-ray Rayleigh fading channel, are simulated. The Rician channel contains one direct path and one Rayleigh fading path with 10-μs time delay between the two paths and equal power in these two paths. The two-ray Rayleigh fading channel contains two Rayleigh fading paths with 10-μs time delay between them and equal power in these two paths. The five-ray Rayleigh fading channel contains five Rayleigh fading paths equally spaced within the time duration of the guard interval and equal power in these paths. The time-variant behaviors of these channels are simulated by using Jake's model [13]. From the simulation results, we can see that the performance of the low-complexity frequency detector can be improved significantly by averaging over several symbols. Fig. 8 shows the error variance of the frequency estimate as a function of the SNR in AWGN channel without frequency offset. We see that the performance of the

TABLE I
THE PARAMETERS OF THE SIMULATED OFDM SYSTEM

Number of subcarriers	1024
Modulation	16-QAM
Total symbol rate	$8 \cdot 10^6$ symbols/s
Symbol period	128 μs
Guard interval	16 μs
Sampling frequency	9 MHz
Signal SNR	10 dB
Frequency offset	0.48 of the subcarrier spacing
Carrier frequency	1.5 GHz
Vehicle speed	100 km/hr

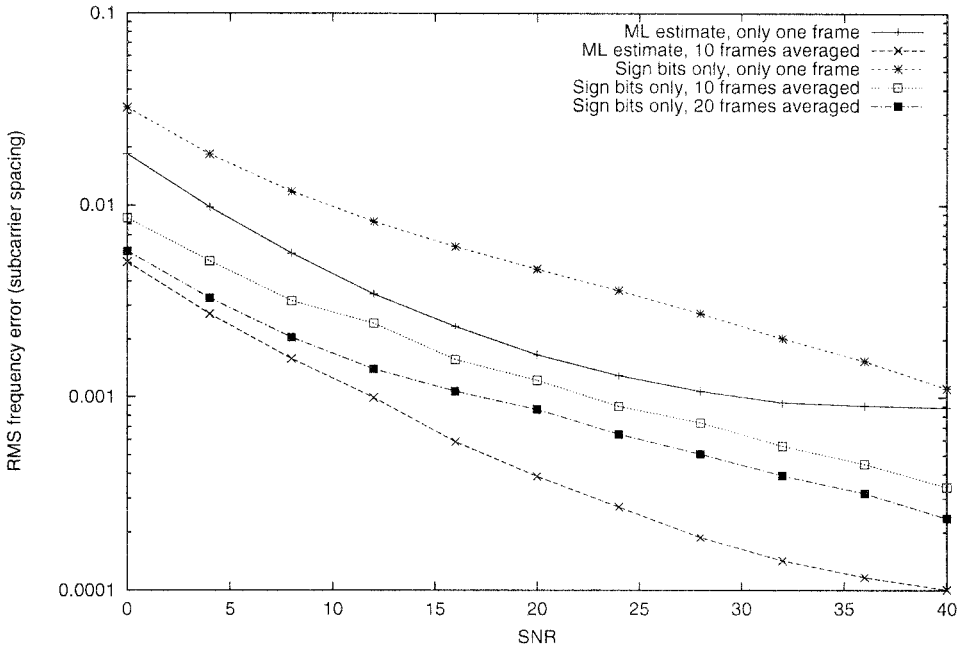

Fig. 8. RMS frequency error as a function of SNR.

maximum-likelihood frequency estimator is also improved by extending the observation interval.

The main impact of the low-complexity frequency detector is the quantization error. We find that the frequency estimation error due to quantization is a function of the frequency offset, as shown in Fig. 9. The quantization effect of the low-complexity frequency detector leads to a floor of residual frequency errors. However, the influence of the quantization errors is small for the frequency offset around zero. This enables us to use a closed tracking loop to compensate the frequency offset as shown in Fig. 1. Fig. 10 shows the performance of the frequency detector in the wireless urban channel used in Section II with various loop gains. The SNR is set to 10 dB in our simulation. We see that the frequency compensator with smaller loop gain has a smaller steady-state frequency jitter, but the acquisition time is longer. In contrast, the frequency compensator with larger loop gain has a shorter acquisition time, but the steady-state frequency jitter is larger. Thus, the selection of the loop gain depends on the Doppler frequency in the channel, the required acquisition speed, and the allowable range of the steady-state frequency jitter. The acquisition time of the closed-loop frequency compensator can be shortened by using unit loop gain for the first frame in order to get a coarse estimate initially, and then switching to a smaller gain to improve the estimate. As shown in Fig. 10, by using this fast acquisition scheme the acquisition time is shortened significantly.

IV. Carrier Frequency Acquisition Scheme

In the GIB frequency offset correction schemes, the applicable range of the frequency offset ϵ is $|\epsilon| \leq 0.5$, that is, $\pm 1/2$ of the intercarrier spacing. The estimate suffers from the subcarrier ambiguity when $|\epsilon|$ is larger than 0.5. A frequency acquisition scheme based on the frequency detector in [4] has been proposed by the authors [11], which can be adopted to the GIB frequency detector easily. The problem of subcarrier ambiguity for $|\epsilon| > 0.5$ can be solved by using the correlation between the received data with frequency offset corrected and the training sequence provided that the autocorrelation function of the training sequence has its maximum at zero. Note that the training sequence used by the frequency acquisition can be the same as the training sequence used by the equalizer. Therefore, no additional specialized sequence is needed and the compatibility of our frequency acquisition scheme is improved. As presented in [11], the frequency acquisition problem of this system can be turned to be a PN sequence acquisition problem. The unknown integral multiple of the intercarrier spacing after the frequency offset correction scheme can be found by shifting the training sequence and correlating it with the received data.

The functional block diagram for the frequency offset correction algorithm with frequency acquisition is shown in Fig. 1. The frequency offset detector estimates the carrier frequency error symbol-by-symbol and feeds the corrected frequency into the receiver and reconstructs the samples. After FFT, we obtain samples that are shifted by an integral multiple of intercarrier spacing. It should be noted that the received samples are corrupted by the channel impairment, which is unknown to the receiver at the synchronization stage. Although the training data is known at the receiver, we still have no information about the channel response of each subchannel. Therefore, an assumption is made on the channel response to eliminate the channel effect on the correlation between the training sequence and the received data. Since the bandwidth of each subchannel is very small in comparison with the overall bandwidth of the OFDM system, the channel responses of neighboring subchannels can be considered virtually the

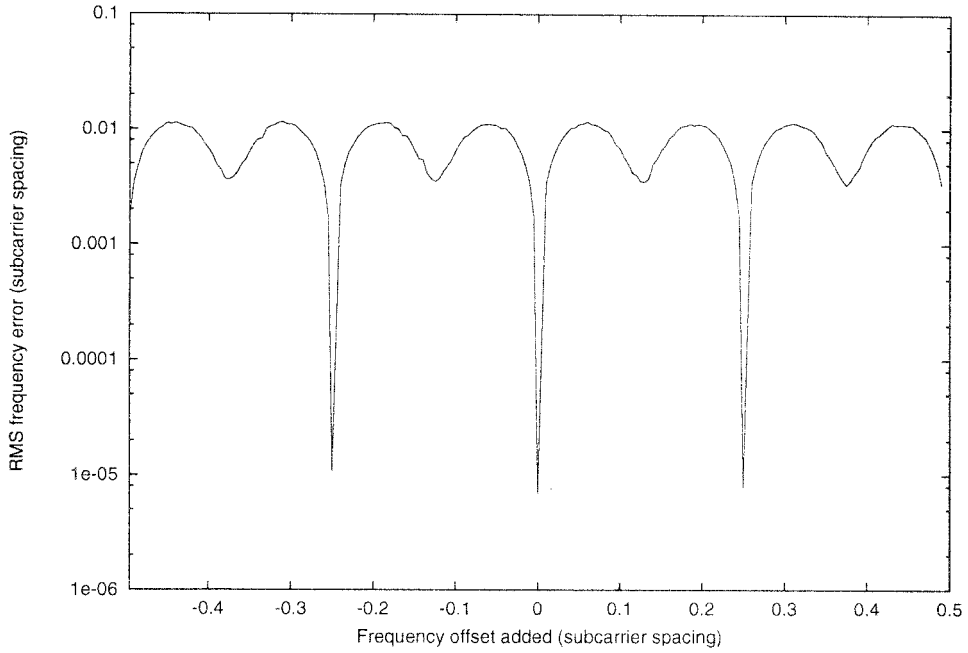

Fig. 9. The estimated frequency error due to quantization for low-complexity frequency detector.

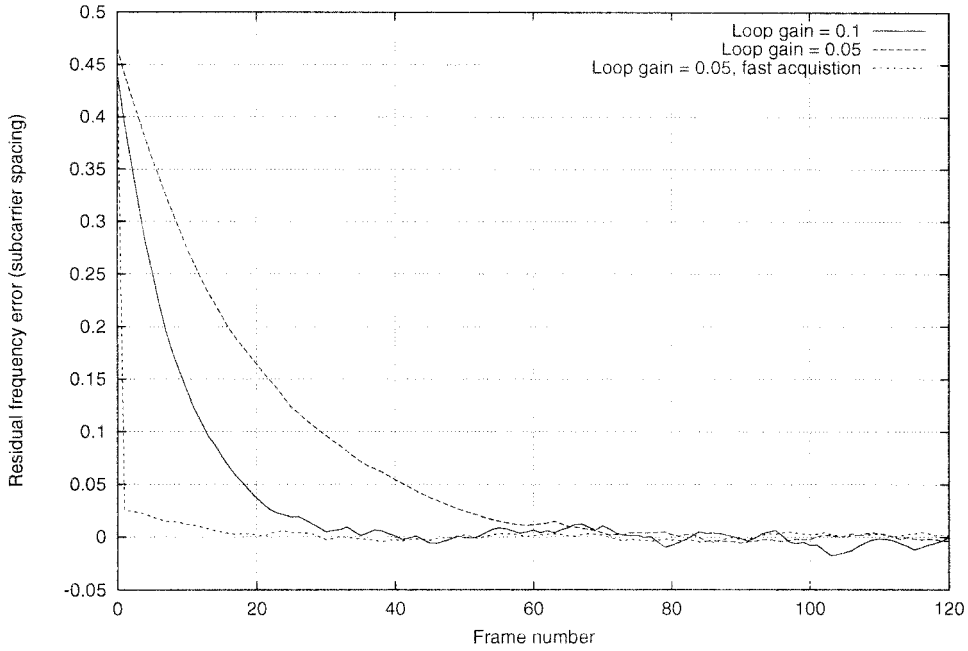

Fig. 10. RMS frequency error as a function of time sample for the closed-loop frequency compensator.

same. A multipath channel model of 20 paths corresponding to the COST-207 urban, nonhilly profile [9] is taken as an example. Let H_k be the channel response of the kth subchannel, and the difference of the neighboring channel response of subchannel k be denoted as $H_k - H_{k+1}$. Fig. 11 shows that the amplitude of the channel difference $|H_k - H_{k+1}|$ is about 10–20 dB lower than the channel amplitude response $|H_k|$ when 1024 subcarriers are used. We also see that the larger the channel response amplitude is, the smaller the subchannel difference will be. This enlightens us to use the data of subchannels with larger channel response to acquire the frequency offset.

Fig. 12 describes the detailed operations of our acquisition scheme. Assuming that, after the frequency correction stage, there still exists a residual frequency error of k_ϵ of the subcarrier spacing and $-P \leq k_\epsilon \leq P$, where P is a positive integer and is denoted as the preset acquisition range. The preset acquisition range P depends on the maximal value of the frequency offset that may occur. The received frequency domain data $\{Y_k\}$ at the FFT output are expressed as

$$Y_k = X_{k+k_c} \cdot H_{k+k_c} + N_k. \tag{16}$$

If a frequency offset occurs, the signals of adjacent channels will interfere the signal in the current channel. For this reason,

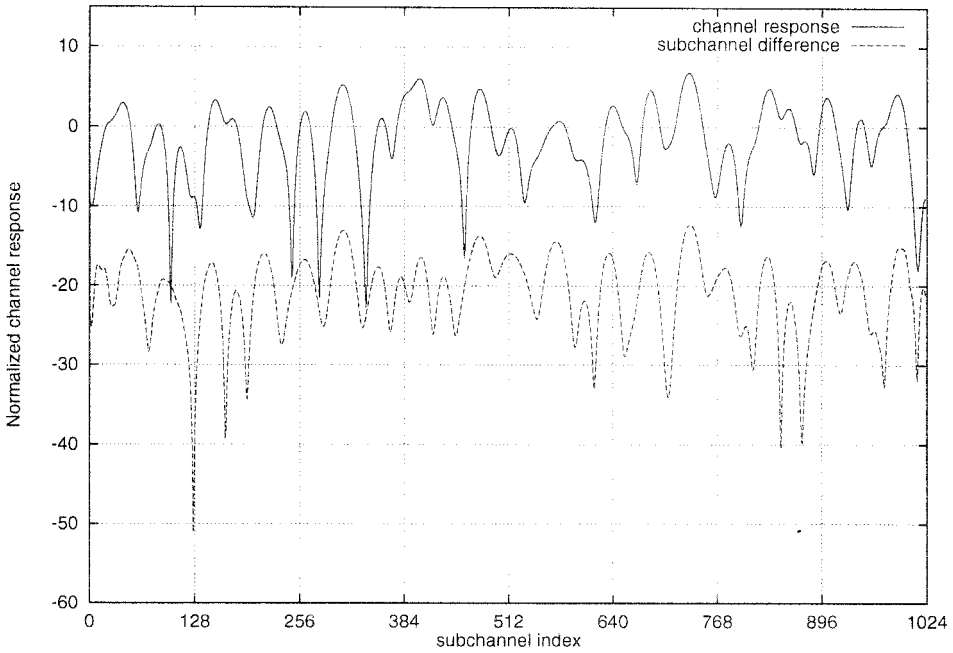

Fig. 11. Multipath channel characteristics with FFT size = 1024.

the subchannels that may be interfered by adjacent channels are discarded when determining the frequency offset. As a result, we confine k in the range of $[-K+P, K-P]$ as shown in Fig. 12. By the above assumption of the channel response, the response of the $(k+k_\epsilon)$th subchannel estimated by

$$\hat{H}_{k+k_c} = \frac{Y_k}{X_{k+k_c}} \tag{17}$$

will be very close to its neighboring subchannel response estimated by

$$\hat{H}_{k+k_c+1} = \frac{Y_{k+1}}{X_{k+k_c+1}}. \tag{18}$$

The frequency offset factor k_ϵ can be obtained by calculating the difference of the channel responses between adjacent subchannels, and therefore the multipath effect can be eliminated. To simplify the hardware implementation, we assess the channel differences by using the sum of the absolute values of the in-phase and quadrature components of channel differences instead of using the mean-squared channel differences. The correlator for the frequency acquisition purpose is devised to average the subchannel differences over $[-K+P, K-P)$ and is denoted as

$$C_j = \frac{1}{2K-2P} \sum_{k=-K+P}^{K-P-1} \left\{ \left| \mathrm{Re}\left(\frac{Y_k}{X_{k+j}} - \frac{Y_{k+1}}{X_{k+j+1}} \right) \right| + \left| \mathrm{Im}\left(\frac{Y_k}{X_{k+j}} - \frac{Y_{k+1}}{X_{k+j+1}} \right) \right| \right\} \tag{19}$$

where $-P \le j \le P$. Evidently, C_j achieves its minimum when $j = k_\epsilon$. As a result, we can estimate the integral frequency offset k_ϵ by searching j over $[-K+P, K-P)$ to obtain the minimum value.

A typical acquisition correlator output C_j as a function of the training sequence shifting index j is shown in Fig. 13. In this simulation, we assume that SNR is 20 dB and the frequency offset is 170 times of the subcarrier spacing and the acquisition range $P = \pm 200$ times of the subcarrier spacing. The response of the multipath channel is shown in Fig. 11. This OFDM system consists of 1024 subchannels, 864 of them are used for data transmission employing 16-QAM. From Fig. 13, we can discern the frequency offset to be 170 times of the subcarrier spacing because the acquisition correlator achieves its minimum when the training sequence shifting index j is 170.

The computational complexity can be evaluated by the iteration number of the acquisition correlator, which depends on the number of the useful subchannels K and the preset acquisition range P. Let M be the iteration number, then

$$M = (2K-2P)(2P+1) = -4P^2 + (4K-2)P + 2K. \tag{20}$$

Fig. 14 shows the normalized computational complexity as a function of the acquisition range. We notice that the theoretical preset acquisition range P can be as large as $K-1$, which is nearly a half of the signal bandwidth. The maximal computational complexity of the acquisition scheme occurs when $P = K/2$. The computational complexity of the acquisition scheme also depends on the modulation method. When QPSK or DQPSK is used, we find that the complex division operations can be reduced to simple phase shifting operations. To further reduce the computational complexity and speed up the correlation process, the partial sum and thresholding technique presented in [11] can be used.

Because of the nonlinear operation in the acquisition operation, it is difficult to assess the missed lock probability

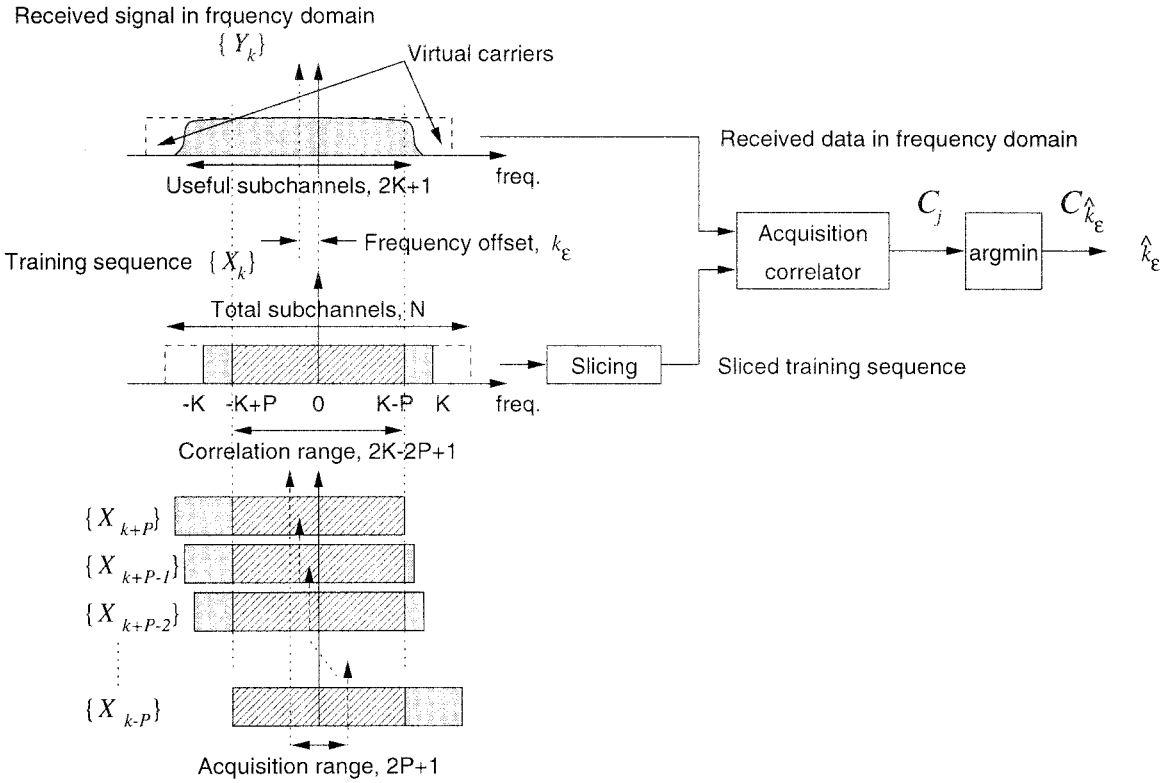

Fig. 12. Frequency acquisition scheme.

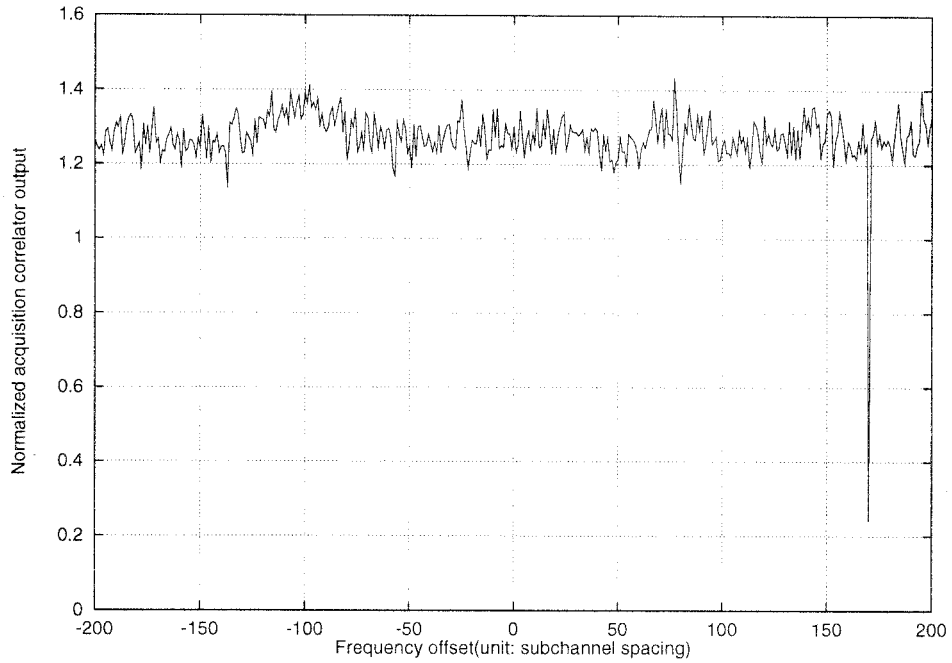

Fig. 13. Frequency acquisition performance under multipath channel with SNR $= 20$ dB, frequency offset $= 170$ of the subcarrier spacing, and preset acquisition range $P = 200$.

P_{ml} analytically. Instead, we assess our acquisition scheme by numerical analysis. Since the missed lock probability of the acquisition scheme is usually very small, it is not efficient to conduct the Monte Carlo simulation. Let $C_{j_{\min}}$ be the minimum of $\{C_j\}$ for $-K+P \le j < K-P, j \ne k_\epsilon$. The proposed frequency acquisition scheme fails when $C_{j_{\min}}$ is smaller than C_{k_c}. Therefore, the missed lock probability P_{ml} of the acquisition scheme is

$$P_{ml} = P[C_{j_{\min}} - C_{k_c} < 0] = P[C_{\text{diff}} < 0] = F_{C_{\text{diff}}}(0) \quad (21)$$

where $C_{\text{diff}} = C_{j_{\min}} - C_{k_c}$ and $F_{C_{\text{diff}}}(x)$ is the cumulative distribution function of C_{diff}. According to the central limit

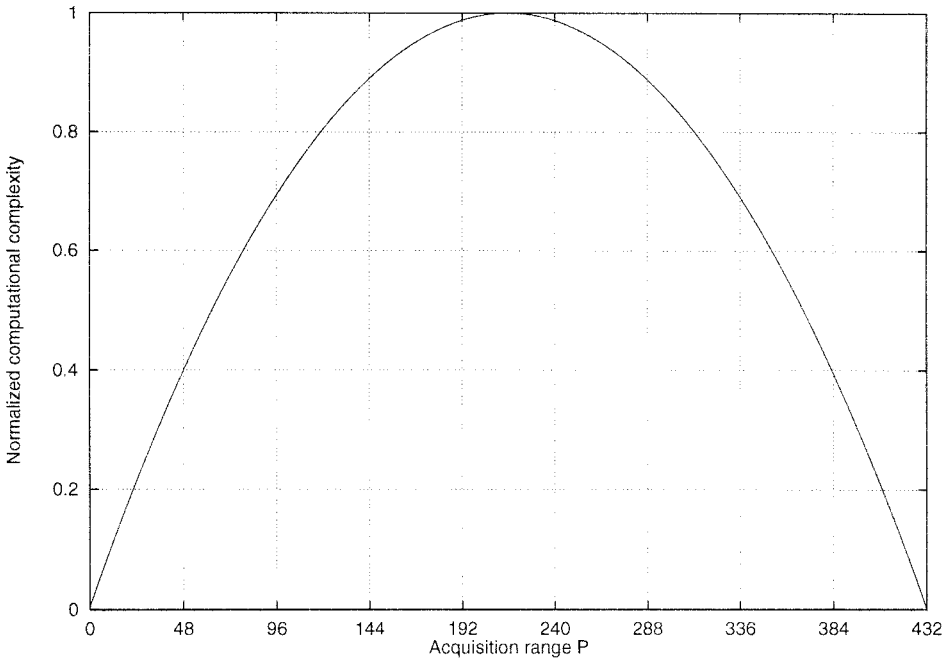

Fig. 14. Computational complexity of the frequency acquisition scheme. 864 out of 1024 subchannels are used.

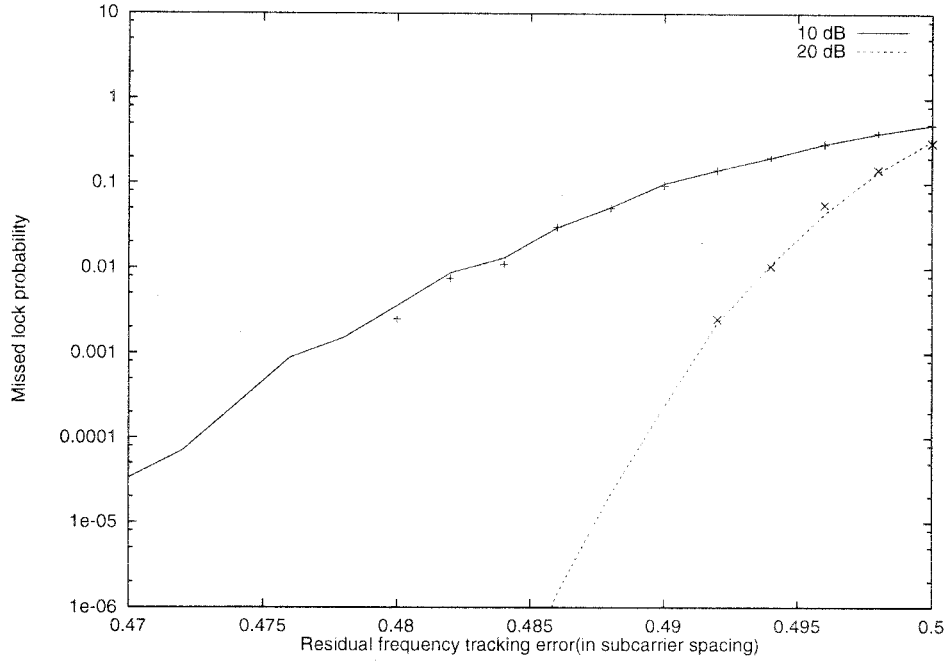

Fig. 15. Acquisition performance versus the tracking error.

theorem, the pdf of C_j is nearly a normal distribution since C_j is a sum of many random variables with the same pdf. Thus, C_{diff} possesses the Gaussian statistics approximately. Then, we obtain the mean μ_{diff} and the variance σ^2_{diff} of C_{diff} from computer simulation, and

$$P_{ml} = F_{C_{\text{diff}}}(0) = \frac{1}{2} \cdot \text{erfc}\left(\frac{\mu_{\text{diff}}}{\sqrt{2}\sigma_{\text{diff}}} \right). \tag{22}$$

In (22), $F_{C_{\text{diff}}}$ is the cumulative distribution function of C_{diff} and

$$\text{erfc}(x) = \frac{2}{\sqrt{\pi}} \int_x^\infty e^{-t^2}\, dt \tag{23}$$

is the complementary error function. Our simulation aims at the multipath channel shown in Fig. 11, and the OFDM system parameters are the same as those in Section III. There are two primary factors that affect the missed lock probability of the

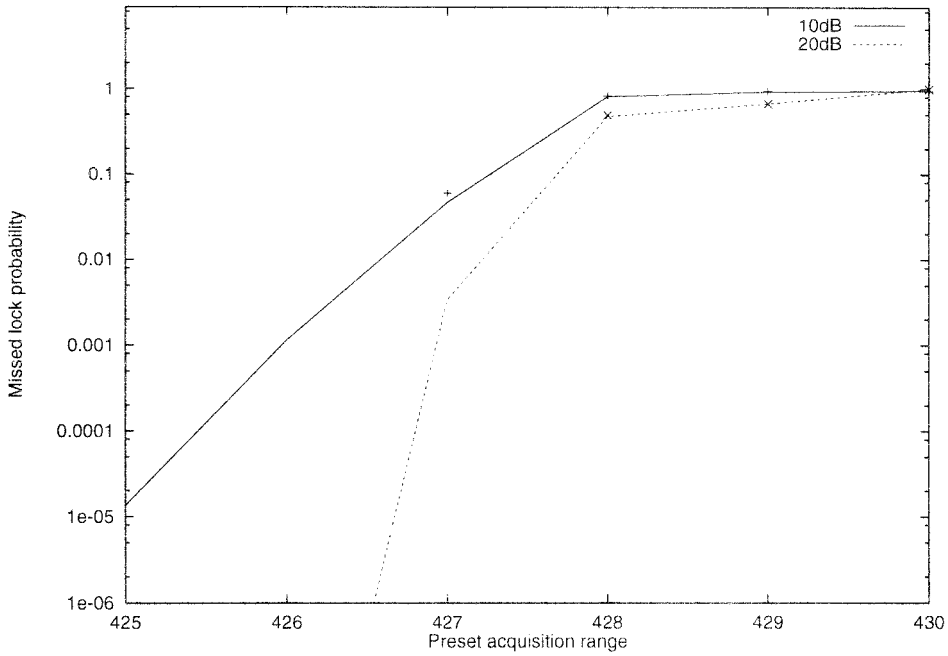

Fig. 16. Acquisition performance versus the preset acquisition range.

acquisition scheme: the residual frequency tracking error and the preset acquisition range P. We investigate these factors by simulations as follows.

A. Residual Frequency Tracking Error

In the acquisition stage, we assume that the residual frequency error after the frequency tracking stage is an integral multiple of the subcarrier spacing. However, there exists a residual frequency tracking error that introduces ICI and degrades the performance of the acquisition scheme. To explore how the residual frequency tracking error affects the acquisition scheme, a computer simulation is taken. Fig. 15 shows the plots of P_{ml} versus the normalized residual frequency tracking error. The solid-line curve and the dashed-line curve represent the P_{ml} estimated by (22) for SNR $= 10$ dB and SNR $= 20$ dB, respectively. In Fig. 15, the "$+$" symbols and the "$\times$" symbols represent the Monte Carlo simulations results for SNR $= 10$ dB and SNR $= 20$ dB, respectively. To speed up our simulation, the acquisition range P is set to ten. We can see that the missed lock probability of the acquisition scheme is still very low even the residual frequency tracking error is as large as 0.47 times of the subcarrier spacing. That is, the proposed acquisition scheme is insensitive to the tracking error. As shown in Fig. 7, the residual tracking error after the frequency detector without averaging process is smaller than 0.15 times of the subcarrier spacing, which is tolerable to the proposed acquisition scheme.

B. Preset Acquisition Range

From (19), we realize that the preset acquisition range P plays an important role in the acquisition scheme. When P is increased, the correlation range will be decreased as indicated in Fig. 12. As a result, the training sequence used to acquire the frequency offset becomes shorter and the autocorrelation property required by the acquisition scheme is more difficult to maintain. Fig. 16 shows the plots of P_{ml} versus the preset acquisition range P for $N = 1024$ and $K = 432$. In Fig. 16, the "$+$" symbols and the "$\times$" symbols represent the Monte Carlo simulation results for SNR $= 10$ dB and SNR $= 20$ dB, respectively. The solid line and the dashed line are the P_{ml} curves estimated by (22) with SNR $= 10$ dB and SNR $= 20$ dB, respectively. From the simulation results, we see that our acquisition scheme performs well even when the preset acquisition range is as large as 425, which is nearly a half of the number of the useful subchannels. From the complexity analysis, we see that the computational complexity of the acquisition scheme is not high when P is close to K. However, for large P, we have to design the training sequence carefully to ensure the autocorrelation property described above.

The acquisition operation of the proposed scheme can be accomplished within one training symbol interval, while the frequency correction scheme in [7] needs several hundreds of FFT block to acquire the frequency offset in $\pm$ten times of the subcarrier spacing due to its small acquisition step. Furthermore, the maximal acquisition range of our acquisition scheme can be extended approximately up to a half of the useful signal bandwidth.

V. Conclusion

In this paper, we have demonstrated how the cyclic extension of OFDM frames can be used to synchronize the frame position and the carrier frequency. Since the estimator uses the inherent information of the OFDM signals, no additional training sequence is needed. We also find that the frame position estimator and the frequency offset estimator are mutually dependent, that is, the frame position and the

frequency offset must be estimated at the same time. In order to reduce the complexity, only the sign bits of the in-phase and the quadrature components of the received OFDM signal are used to estimate the frame position and the frequency offset. It is also found that if we average our estimate over several consecutive OFDM symbols, we obtain a similar performance as the estimate without quantization. From the computer simulations, we find that the new estimator works well under fading channels. For the cases whose frequency offset is larger than $\pm 1/2$ of the subcarrier spacing, we propose a frequency acquisition scheme to estimate the additional frequency offset based on the assumption that the difference of the frequency response of the neighboring subchannels is very small. The training sequences used by our frequency acquisition scheme can be the same as the training sequences used by the equalizer, and, therefore, no additional modification is needed in the transmitter.

REFERENCES

[1] J. A. C. Bingham, "Multicarrier modulation for data transmission: An idea whose time has come," *IEEE Commun. Mag.*, vol. 28, pp. 5–14, May 1990.

[2] W. D. Warner and C. Leung, "OFDM/FM frame synchronization for mobile radio data communication," *IEEE Trans. Veh. Technol.*, vol. 42, pp. 302–313, Aug. 1993.

[3] J.-J. van de Beek, M. Sandell, M. Isaksson, and P. O. Borjesson, "Low-complex frame synchronization in OFDM systems," in *Proc. IEEE Int. Conf. Universal Personal Commun.*, Toronto, Canada, Sept. 27–29, 1995, pp. 982–986.

[4] P. H. Moose, "A technique for orthogonal frequency division multiplexing frequency offset correction," *IEEE Trans. Commun.*, vol. 42, pp. 2908–2914, Oct. 1994.

[5] F. Daffara and A. Chouly, "Maximum likelihood frequency detectors for orthogonal multicarrier systems," in *Proc. IEEE Int. Conf. Commun.*, Geneva, Switzerland, May 23–26, 1993, pp. 766–771.

[6] F. Daffara and O. Adami, "A new frequency detector for orthogonal multicarrier transmission techniques," in *Proc. IEEE Veh. Technol. Conf.*, Chicago, IL, July 25–28, 1995, pp. 804–809.

[7] F. Classen and H. Meyr, "Frequency synchronization algorithms for OFDM systems suitable for communication over frequency selective fading channels," in *Proc. IEEE Veh. Technol. Conf.*, Stockholm, Sweden, June 8–10, 1994, pp. 1655–1659.

[8] H. Nogami and T. Nagashima, "A frequency and timing period acquisition technique for OFDM systems," in *Proc. IEEE PIMRC*, Toronto, Canada, Sept. 27–29, 1995, pp. 1010–1015.

[9] *Digital Land Mobile Radio Communications—COST 207.* Brussels, Luxembourg: Commission of the European Communities, 1989.

[10] M. Okada, S. Hara, S. Komaki, and N. Morinaga, "Optimum synchronization of orthogonal multi-carrier modulated signals," in *Proc. IEEE PIMRC*, Taipei, Taiwan, Oct. 15–18, 1996, pp. 863–867.

[11] M. H. Hsieh and C. H. Wei, "A frequency acquisition scheme for OFDM systems," in *Proc. IEEE PIMRC*, Taipei, Taiwan, Oct. 15–18, 1996, pp. 843–847.

[12] M. Luise and R. Reggiannini, "Carrier frequency acquisition and tracking for OFDM systems," *IEEE Trans. Commun.*, vol. 44, pp. 1590–1598, Nov. 1996.

[13] W. C. Jake, *Microwave Mobile Communications.* New York: Wiley, 1974.

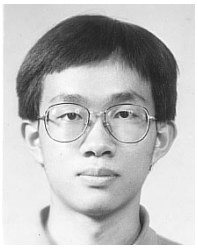

Meng-Han Hsieh (S'97) was born in Taiwan, R.O.C., in 1968. He received the B.S. and M.S. degrees in electronics engineering from National Chiao Tung University, Hsin Chu, Taiwan, in 1990 and 1992, respectively. He is currently working toward the Ph.D. degree at National Chiao Tung University.

His research interests include synchronization and channel estimation algorithms for multicarrier transmission systems.

Che-Ho Wei (S'73–M'76–SM'87–F'96) was born in Taiwan, R.O.C., in 1946. He received the B.S. and M.S. degrees in electronics engineering from National Chiao Tung University, Hsin Chu, Taiwan, in 1968 and 1970, respectively, and the Ph.D. degree in electrical engineering from the University of Washington, Seattle, in 1976.

From 1976 to 1979, he was an Associate Professor at National Chiao Tung University, where he is now a Professor in the Department of Electronics Engineering. From 1979 to 1982, he was the Engineering Manager of Wang Industrial Company, Taipei, Taiwan. He was the Chairman of the Department of Electronics Engineering of National Chiao Tung University from 1982 to 1986 and Director of the Institute of Electronics from 1984 to 1989. He was on leave at the Ministry of Education and served as the Director of the Advisory Office from September 1990 to July 1992. His research interests include digital communications and signal processing and related VLSI circuits design.